

Spatial distribution of waves and wave-induced littoral drift along the nearshore regions of the central west coast of India

Jesbin George^{1,2}, V. Sanil Kumar^{1*}, Duphrin Joseph¹

¹Ocean Engineering, Council of Scientific and Industrial Research-National Institute of Oceanography, Dona Paula, Goa - 403 004 India

²Department of Marine Science, Bharathidasan University, Tiruchirappalli, India

*Corresponding author email: sanil@nio.org; Tel: 0091 832 2450327

Abstract

The spatial distribution of nearshore wave characteristics and wave-induced littoral drift along the Central West Coast of India (CWCI) is investigated using a wave transformation model. Previous approaches in littoral drift estimations along the CWCI were based on single-point data, and the spatial distributions of littoral drift patterns along the CWCI were not attempted. A new approach has been implemented, where time and space varying measured wave data is used as an input to the model, collected at ~15 m water depth at three locations in the CWCI. The model results are compared and validated with the measured wave data at 9 and 5 m during the monsoon and non-monsoon period. On an annual scale, along the CWCI, the significant wave height varies from 0.8 to 1.2 m, the period in the range of 4-6 s, and the predominant direction is southwest-west (~230-270°). The study also examines alongshore varying energy fluxes in the CWCI. In the breaker zone along CWCI, wave height varies up to 18% during non-monsoon, while the period and direction vary less than 10%, and during monsoon, these variations are less than 7%. The present study also examines the spatial distribution of littoral drift along four selected stretches. A predominant southerly net drift is observed among most regions of CWCI. We also estimated the littoral drift during calm, monsoon, and cyclone conditions. It is observed that cyclone events that lasted for a few days generated ~ 40% of the LST generated during an entire pre-monsoon season.

Keywords: nearshore waves, longshore sediment transport, coastal processes, nearshore modeling

1. Introduction

Thorough knowledge of nearshore wave characteristics is essential for coastal engineering applications and understanding the coastal processes. The wave characteristics are important determiners for coastal designs, sustainable coastal management (Odériz et al., 2020) and play a pivotal role in shaping the morphological evolution of coasts. The onshore propagating nearshore waves dissipate their energy in the surf zone and initiate Longshore Sediment Transport (LST), also termed as littoral drift, driven by the longshore current produced by the breaking waves obliquely approaching the coast (Longuet-Higgins, 1970). LST is one of the main factors influencing coastal geomorphology (Kamphuis, 1991), and its reliable estimation is a fundamental requirement for coastal engineering applications in the coastlines worldwide (McCarroll et al., 2019). Hence, it is equally important to understand the region's nearshore characteristics and LST to protect its coastlines effectively.

The west coast of India, having many harbours, ports, and estuaries, has become an area of interest due to its rapidly growing socio-economic developments (Chowdhury and Behera, 2017). The wave climate in this region, which forms a part of the eastern Arabian Sea, is very dynamic since it experiences a seasonal reversal of wind system associated with the monsoon (Anoop et al., 2015), where strong southwest winds blow over this region during June-September. Significant wave height up to 6 m is previously reported off Goa at 23 m water depth in the eastern Arabian Sea during the monsoon (Kumar et al., 2006). It is very well documented that the wave climate of the eastern Arabian Sea is influenced by the Findlater Jet in the monsoon (Anoop et al., 2015; Kumar and George, 2016), swells propagating from the tropical Indian Ocean and the Southern Ocean (Amrutha et al., 2017; George and Kumar, 2020) and the Shamal (Aboobacker et al., 2011) and Makran winds (Anoop et al., 2020).

The Central West Coast of India (CWCI, Figure 1) contains several open sandy beaches (Chandramohan et al., 1993) and are directly exposed to the high energetic waves (both swells and wind-seas) during the monsoon, followed by low energetic/long-period swells in the non-monsoon period (George and Kumar, 2020). Based on the monthly beach profiles measurements, Chandramohan et al. (1993) and Kumar et al. (2001) observed seasonal changes without annual net erosion at few beaches of the CWCI. Most of the beaches along the CWCI are undergoing seasonal erosion, and most among them regain the maximum profiles from February to April. The distribution of longshore current direction is not uniform along the CWCI, indicating the presence of a variable littoral transport environment. This region is subjected to relatively low wave energy during the non-monsoon period. Kankara et al. (2018), using satellite images, observed that 24, 12, and 22% of shorelines along the Maharashtra, Goa, and Karnataka states in CWCI are eroding, while 12, 20, and 30% of their shorelines

are accreting. Long-term LST rates at few locations along the CWCI using re-analysis datasets and modeling approaches suggested a gross northward transport in LST rates (George and Kumar, 2019 and Chowdhury and Behera, 2017). Hence, understanding the nearshore wave climate and morphological changes associated with them along the CWCI is of great interest to the coastal managers, as the nearshore regions up to 10 km from the coast along the CWCI are intense fishing zones and are extensively used for tourism-related activities and development of marine facilities (George et al., 2020).

Numerous studies in the past, using re-analysis data (e.g., Anoop et al., 2014; George and Kumar, 2019; Shanas and Kumar, 2014a) and measured wave data (e.g., Amrutha et al., 2016b; Noujas et al., 2018) has examined the temporal variations in the wave characteristics and LST rates along selected locations in the CWCI. Variations in the wave characteristics across selected sites in the central west coast using measured wave data were also examined by a few (Anoop et al., 2014; Kumar et al., 2012). To the author's knowledge, no studies were previously attempted along the entire stretch of the CWCI, which employs a wave transformation numerical model with simultaneously measured wave data for one year period at many locations as input to examine the spatial distribution of nearshore wave characteristics and LST rates. Thus, the present study aims to understand more about the distribution of wave characteristics and LST rates, particularly along the nearshore regions of the CWCI. We also analyzed the alongshore varying wave characteristics and energy fluxes at 10 m water depth along CWCI. The paper is arranged as follows. Section 2 gives information about the data and methods used for the present study. The results and discussion are addressed in section 3, followed by conclusions in section 4.

2. Data and methodology

The bathymetry of the study domain is obtained by digitizing the recent national hydrographic charts (Chart Nos. 213, 256, 2038, 2041, 2042, 2043, and 2077) for water depths up to 20 m. The wave data is measured using MK-III Datawell directional wave rider buoys (Barstow and Kollstad, 1991), deployed at ~15 m water depth during January-December 2017 for every 30-minute interval at three locations (Ratnagiri, Vengurla, and Karwar) in the CWCI and is used as the input in the wave transformation model (Figure 1). The distance between Ratnagiri to Vengurla is ~ 130 km, and Vengurla to Karwar is ~140 km. Input wave parameters to the model are significant wave height (H_s), wave period, mean wave direction, and directional spreading. Delft3D Wave module (Hydraulics, 2006) is used as the numerical model for nearshore wave transformation and was successfully employed earlier at specific locations in the CWCI (George et al., 2020, 2019; Shanas and Kumar,

2014b). The wave transformation is based on a third-generation wave model SWAN (Booij et al. 1999), and the governing equation is given below as,

$$\frac{\partial}{\partial t} N + \frac{\partial}{\partial x} C_x N + \frac{\partial}{\partial y} C_y N + \frac{\partial}{\partial \sigma} C_\sigma N + \frac{\partial}{\partial \theta} C_\theta N = \frac{S}{\sigma} \quad (1)$$

Where, N is the action density spectrum, θ and σ are the wave direction and the wave relative frequency, respectively. The first term in the equation indicates the rate of change of action density in time. The second and third term is the propagation of action in geographical space. The fourth term denotes the shift in relative frequency, and the fifth terms indicate refraction for both depth and current. The source term of energy density (S) is shown on the right-hand side and is expressed as

$$S = S_{in} + S_{ds} + S_{nl} \quad (2)$$

S_{in} is the generation of wave energy by wind, S_{ds} is the dissipation of wave energy through white-capping, bottom friction, and depth-induced wave breaking, and S_{nl} is the energy transfer due to nonlinear wave interaction. Other input variables are the bottom friction coefficient (taken as $0.067 \text{ m}^2/\text{s}^3$) as suggested by Hasselmann et al. (1973), alpha (1), and gamma (0.73) for depth-induced breaking (Battjes and Stive, 1985). The grid generation is done with ‘RGFGRID’ of the Delft3D-WAVE module. The model has 10° directional resolution and has 24 frequencies ranging from 0.05-1 Hz.

Four sandy beaches along the CWCI are chosen for the study. The selected stretches are Ganpatipule, Vengurla, Karwar, and Honnavar (Figure 1). Ganpatipule coast is located in the Ratnagiri district of Maharashtra with a gentle beach slope ($>1:50$), having fine to medium grain size sediment varying from 0.125-0.5 mm (Sharma et al., 2017). Vengurla coast, located in south Maharashtra, is a typical pocket beach of about 5 km stretch. Karwar coast is located in north Karnataka, attached to few offshore/nearshore islands, and the beaches lie in a wave-dominated micro-tidal estuarine environment (Dora and Kumar, 2018). Honnavar coast is located ~ 70 km south of Karwar, and it lies north of the Sharavati river mouth. The average tidal range of the study region is 0.6 m during neap tide and 2 m in spring tide.

The study domain (~ 336 km stretch, Figure 2a) is first divided into a large rectangular grid of 300×580 grid points with a spacing of 142 m and 580 m along the x and y directions, respectively. Four high-resolution rectangular grids of 24 m spacing (each for both x and y directions) is also created along the selected stretches in the study domain, i.e., Ganpatipule (132×384 , Figure 2b), Vengurla (119×233 , Figure 2c), Karwar (246×264 , Figure 2d) and Honnavar (174×408 , Figure 2e). These four high-resolution grids are nested into the larger grid with lower resolution. The model is assigned

with the following boundaries, i) an open boundary to the west, which is further divided into three segments (Figure 1, A-B, B-C, and C-D) where time-varying and space varying conditions are applied along each segment, ii) lateral boundaries to the north and south, and iii) closed boundary to the east. To compare and validate the model results, measured wave data during a non-monsoon month (April) at 5 m water depth and monsoon month (June) at 9 m water depth off Honnavar is used. The model's performance is determined by comparing model and measured data using statistical approaches such as bias, root-mean-square error (RMSE), and correlation coefficient (R). The transformed wave characteristics are extracted from 4 m water depth to understand the nearshore characteristics along the selected stretches. Wave characteristics along 10 m water depth contour are extracted to examine the alongshore varying wave characteristics and energy fluxes. The LST rate is estimated using equation (1) suggested by CERC (USACE, 1984), and wave energy flux is computed using equation (2).

$$Q = 0.023 \sqrt{\frac{g}{K_i}} H_b^{2.5} \sin 2\theta \quad (1)$$

$$P = \frac{1}{8} \rho_w g H_b^2 C \sin(\theta) \cos(\theta) \quad (2)$$

Where, Q is the LST in volume per unit time, P is the alongshore wave power (W/m), H_b is the breaking wave height (m), g is the acceleration due to gravity (9.81 m/s²), ρ_w is the density of water (1030 kg/m³), C is the wave speed, θ is the angle between breaking wave crest and local shoreline (deg), and K_i = a constant (0.78).

3. Results and Discussion

3.1 Model validation and comparison

The model results are compared with measured data (Figure 3). It is evident from the figure that the model gives a good comparison with the measured data. During the non-monsoon period, at 5 m depth, H_s gives an R-value of 0.83, a bias of 0.09 m, and RMSE of 0.12 m, whereas, during monsoon at 9 m depth, R, bias, and RMSE are 0.89, -0.05 m, and 0.25 m indicating that the model has replicated the H_s conditions in the nearshore waters adequately during both the seasons. The mean wave period estimate during both seasons are also good. During the non-monsoon period, the R, bias, and RMSE values are 0.75, 0.53 s, and 0.76 s, whereas, during monsoon, they are 0.81, -0.07 s, and 0.5 s, respectively. However, few cases are observed where the long-period waves, particularly during the non-monsoon period, are underestimated by the model with a bias of nearly 2 s. Previous simulations (SWAN model nested in WAVEWATCH III) along the CWCI at Karwar (Amrutha et al., 2016a) also reported an underestimation (~31%) of the mean wave period during the non-monsoon period. The

model replicated the mean wave direction from the south-southwest ($\sim 220-240^\circ$) and the north-northwest ($270-290^\circ$) during the non-monsoon period. However, instances where the model fails to capture these waves are also observed, where the model under-predicts the north-northwest waves and over-predicts south-southwest waves during non-monsoon. The inefficiency of replicating north-westerly waves in the wave transformation model along the central west coast was previously reported by George and Kumar (2019) and George et al. (2020). The R, bias and RMSE values are 0.52, 1.9° , and 14° during the non-monsoon period. During monsoon, the wave direction generally oscillates in the range of $250-260^\circ$, and for a few times, the model under-predicts or over-predicts, giving rise to poor correlations ($R = 0.32$). The bias and RMSE values during monsoon are 5.8° and 9.9° , respectively. Along the Vengurla coast in the CWCI, George et al. (2020) has also reported similar variations in the wave directions in the wave transformation model and also reported significant differences in the direction of wind-seas and swells at 15 m and 5 m water depths due to the co-existence of wind-seas and swells having equal magnitude.

3.2 Wave characteristics along the CWCI and at selected stretches

The averaged wave characteristics along the CWCI during different seasons and on an annual scale are discussed here (Figure 4). During pre-monsoon, the H_s varies from 0.1–0.8 m along the CWCI. The southern and the northern part generally experiences slightly higher intensity H_s (0.6-0.8 m) than the central domain (0.4-0.6 m). This can be attributed to the co-existence of swells and wind-seas in the Arabian Sea, where the predominance of more southern/south-westerly swells (north-westerly wind-seas) in the southern (northern) part of the study domain leads to the resultant increased H_s . During this season, the mean wave period generally varies in the range of 4-5 s across the whole domain, followed by waves from the northwest ($260-280^\circ$) in the northern part and south-southwest waves ($220-260^\circ$) in the central to the southern region. These northerly waves along the northern part are due to the shamal and Makran winds, and their intensity reduces from north to south (Aboobacker et al., 2011; Anoop et al., 2020). The waves approaching from the south-south-west direction would be the Southern Ocean/south Indian Ocean swells (Remya et al., 2020; George and Kumar, 2020). When the Indian summer monsoon approaches, the domain experiences an increased H_s (varying from 1-2 m) and an increased period (varying from 6-7 s) in the southern and central part, while along the northern region, the period is slightly less (ranges from 5-6 s). During this period, the mean wave direction generally varies in the range of $250-260^\circ$ in almost all parts of the domain. However, along the nearshore regions, particularly along the central to the southern part, it ranged from $230-250^\circ$. As the monsoon withdraws, the southern part experiences slightly higher waves (0.6-0.8 m) than the central and northern domains (0.4-0.6 m). The wave period along the study domain varies from 4-6 s

during this season. The direction during this season generally varies in the range of 230-240° along the southern and central domains, whereas, in the northern region, the direction is 250-260°. Annually, across the study domain, the Hs varies in the range of 0.8-1.2 m, with a period of 4-6 s and direction 230-270°.

To examine the behavior of seasonal and annual averaged wave characteristics in the nearshore waters, four locations in CWCI are selected (Figure 5). The locations are Ganpatipule, Vengurla, Karwar, and Honnavar, and their nearshore (at 4 m water depth) wave characteristics is also examined (Figure 6a-i). The seasonal averaged Hs and period range distributed along the four stretches and their predominant wave directions during each season are shown in Table 1. All four stretches experiences Hs < 1 m on average during non-monsoon months. The mean wave period values distributed along the four stretches are similar during all the seasons, except along the Ganpatipule coast, which experiences lower period waves during the post-monsoon season (Table 1, Figure 5a). Waves typically approach the coast of Ganpatipule from 226-316° during pre-monsoon (Figure 6c), where predominant waves (~53% of the time) are from the south-southwest (226-255°, Table 2). However, the predominant wave direction (~54% of the time) during monsoon oscillates between 250 and 260°. On an annual scale, the entire domain experiences Hs in the range of 0.7-1.0 m, period 4-6 s, and direction 220-280° with predominant wave direction in the range of 250-260° (Figure 5a). More than 64% of the waves approach from the south-southwest direction (>255°) in the nearshore waters. Previous modeling approaches along the Ganpatipule region based on measured (George et al., 2019) and re-analysis (George and Kumar, 2019) data also suggest similar breaker heights and periods along the region. However, the prevailing wave conditions observed by them were in the range of 220-250° during the non-monsoon period, whereas the present study indicates that the direction oscillates between 240 and 260°.

Along the Vengurla coast (Figure 5b), the annual averaged Hs varies from 0.7-1.0 m, and along the nearshore regions during pre and post-monsoon, the waves are from the south-southwest direction (< 248°) for most of the time (~85%). The periods observed along the region (Tables 1 and 2) are similar to the previously observed mean wave period across the domain during 2016 (Amrutha et al., 2016b). The direction generally oscillates between 220 and 260° for the whole domain during pre and post-monsoon. During monsoon, the direction in the nearshore regions generally oscillates between 245-255° (~66% time). The observed nearshore wave characteristics are consistent with the previously reported characteristics in the domain (e.g., George et al., 2020; Noujas et al., 2018).

Along the Karwar (Figure 5c), on an annual scale, the Hs ranges between 0.4 and 1.2 m. Annually, the wave period in the nearshore region ranges from 2.7-9.6 s with an averaged value of 5.1

s (Figure 6g). During all the seasons, the direction across the domain varies in the range of 220-300°, while the predominant wave direction during monsoon and the annual average is 240-250° (Figure 5c, Table 1). However, in the island-sheltered regions in the southern part of the domain, wave direction is $> 270^\circ$. Dora and Kumar (2018, 2015) based on modeling approaches reported that the nearshore islands, named Kurmagadgudda and Shimisgudda, play a pivotal role in the variation of breaking wave intensity along Karwar. The observed southerly waves are the result of interference between the waves diffracted due to the presence of these islands (Dora and Kumar, 2018). In the nearshore waters, ~75% time, south-southwest waves ($\sim 255^\circ$) are observed during the non-monsoon season, while 80% of times during monsoon, the direction oscillates between 245 and 260° (Figure 6i, Table 2).

Along the Honnavar region (Figure 5d), annually, H_s range from 0.1-1.1 m. Lower H_s (< 0.15 m) are observed in the Sharavati river mouth during all seasons. In the nearshore regions, H_s annually varies from 0.2-1.9 m with an average value of 0.9 m (Figure 6j), period ranges from 2.8-9.5 s with an average value of 5.2 s (Figure 6k). During the non-monsoon seasons, south-southwest waves ($< 243^\circ$) approach the shore more than 74% of the time. However, the predominant direction during monsoon is from 250-260° across most parts of the domain, and the direction oscillates in the range of 242-255° during ~83% of the time in the nearshore zone (Table 2). The observed wave characteristics are similar to the values reported by Chempalayil et al. (2014).

Variations in the nearshore wave characteristics along the selected four locations are discussed here. Anoop et al. (2014), based on measured and re-analysis data sets, observed that the wave characteristics were similar ($< 10\%$ variation) for a 270 km stretch along the CWCI (Karwar to Ratnagiri) during the monsoon since the waves along this domain are predominantly swell waves. They also reported a higher spatial variation ($> 20\%$) in wave characteristics during the non-monsoon period. Also, Kumar et al. (2012), based on measured wave data of three stations covering 200 km along the Karnataka coast, reported that seasonal averaged wave height and period did not vary significantly. The present study shows that during the non-monsoon season, H_s in the nearshore zone varies up to 18%. The nearshore regions of Vengurla experience lower H_s compared to the other areas. The difference in the intensity of H_s along the northern and southern parts of the domain is relatively very low ($< 3\%$). The period and directions vary less than 10% in the nearshore zone of selected stretches during the non-monsoon period, and during the monsoon, the variations are less than 7% in the nearshore regions.

3.3 Alongshore varying wave characteristics and wave energy fluxes

The alongshore wave characteristics in the nearshore regions (~10m water depth) of CWCI are extracted (Figure 7). H_s reach up to 3.8 m along the domain during monsoon, whereas during other non-monsoon months, H_s vary from 0.2-1.5 m. Compared with other regions, during the non-monsoon period, lower H_s values are observed along the central domain. However, in response to the Ockhi cyclone (A very severe cyclonic storm with the highest wind speed of 185 km/h) during the first week of December, the CWCI experienced larger H_s (ranging from 1.5-2.5 m). Even though it is a well-known fact that during monsoon and cyclone periods, wave heights will be much higher than the calm period, a comparison of maximum H_s (MHs) occurred along the domain for seven days during the three conditions is done (Figure 8a), to examine the variations and behaviour of MHs along the entire CWCI during these conditions. In most of the southern and central region, the MHs is in the range of 2.0-2.4 m, while in the northern part it ranges from 2.2-2.4 m. A sudden decline in the MHs is observed for all the three conditions along the central part of the domain (~ near to Karwar) due to the presence of several small islands in the region (Dora and Kumar, 2015), resulting in irregularity in bathymetry and the wave characteristics (Figure 7). During monsoon, MHs vary in the range of 2.6-3.6 m along the domain and in most regions, MHs show a larger variation (~47%) compared with the calm condition (Figure 8a). However, during the cyclone Ockhi event, MHs variations are negligible (~2%) along the domain compared to calm conditions. This implies that the MHs along the nearshore regions of CWCI is larger during the monsoon than during the Ockhi cyclone period. In 2019, the Kyarr cyclone (a super cyclonic storm with the highest wind speed of 240 km/h) formed in the Arabian Sea, and its impact on the nearshore waters (at 4m water depth) along the Vengurla domain is shown in Figure 8b. The H_s reaches up to 2 m in nearshore waters during both the monsoon and cyclone Kyarr events in 2019.

Most of the time, the mean wave period (Figure 7) varies from 2-6 s along the whole domain during the non-monsoon months. During some instances, the mean wave period exceeds this range, particularly along the southern part of the domain (exceeds up to 9 s) due to the presence of the Southern Ocean/south Indian Ocean swells in the eastern Arabian Sea (Amrutha et al., 2016; George and Kumar, 2020). During the monsoon, the wave period is in the range of 4-8 s, and most of the time, the wave period is in the range of 6-8 s. During the cyclone event, the wave period is in the range of 6-8 s, and previously Kumar et al. (2019) reported the mean wave period of ~8.9 s along the Mumbai coast during the Ockhi cyclone. The mean wave direction at 10 m water depth varies from 210° - 330° across the domain. As discussed in the previous section, the presence of north-westerly waves

(direction $> 270^\circ$), particularly along the northern part, and the presence of southerly swells (direction $< 240^\circ$) along the central and southern region during the non-monsoon month are more evident from here. During monsoon, the waves generally approach the coast from 240° - 270° .

The wave characteristics at 10 m water depth can provide a first-order proxy for the direction of LST at a regional scale, as LST is the consequence of wave stirring and subsequent transport by the longshore current (Anderson et al., 2018). Hence, alongshore varying energy fluxes along the CWCI are computed using equation 2 (Figure 7). Along most parts of the domain, the energy fluxes generally vary from -8000 to 8000 W/m. Predominantly, southerly directed energy fluxes are observed in the northern part of the domain in response to the north-westerly waves during non-monsoon months, followed by northward directed energy fluxes in the central and southern parts in response to the southerly/south-westerly swells. However, large southerly directed energy fluxes are observed during monsoon in the south and central regions where the rate is more than 20000 W/m.

3.4 Longshore sediment transport rate along the selected stretches

LST rate (LSTR) along the four stretches is computed using the CERC equation (Eq. 1), and the gross and net LST ranges for the four stretches are shown in Table 3. Predominantly, a southerly drift is observed along most parts of the Ganpatipule region (Figure 9a), except along few portions in the north and central areas where the drift is towards the north. The present LSTR estimated along the Ganpatipule (Table 3) is comparable with the previously reported LSTR using visual observation and measured data (Chandramohan et al., 1993, George et al., 2019). However, using re-analysis data (ERA-Interim), a long-term investigation of LSTR was estimated by George and Kumar (2019) and Chowdhury and Behera (2017), which is larger (ranging from 2 to $8 \times 10^5 \text{ m}^3$) than the present study. This larger difference between the LST estimated in the present study using measured data versus the ERA-Interim input is due to the latter's coarse resolution, both spatially and temporally. Thus, the source of the wave data used in the model input plays a pivotal role in reducing the uncertainties in estimating LSTR.

Along the Vengurla coast (Figure 9b), larger values are observed along the northern part of the region where the net drift is directed northward ($\text{LSTR} > 0.9 \times 10^5 \text{ m}^3$) in comparison with the southern part of the domain, which has a southerly drift ($\sim 0.4 \times 10^5 \text{ m}^3$). A southerly transport rate along this region was previously reported by Chandramohan et al. (1993). Using the LITDRIFT model, Noujas et al. (2018) estimated a gross transport rate of $1.18 \times 10^5 \text{ m}^3$ along this region and suggested that the annual net LSTR along the domain is relatively less (varies from -7778 to -9015 m^3). The gross LSTR estimated in the present study agrees with the previously reported LSTR along the domain (Noujas et

al., 2018, Chandramohan et al., 1993). However, previous studies reported predominant southerly drift in the domain. In contrast, the present study observed a large northward drift in the northern part of the domain followed by a reduced southerly drift in the southern and central part of the domain. In general, most regions along the Vengurla experiences a northward drift. A recent study (George et al., 2020) based on a wave transformation model with measured data during September 2014-August 2018 as input has also observed a northward net drift in the LST along the Vengurla coast.

Along Karwar (Figure 9c), large (LSTR $> 0.7 \times 10^5 \text{ m}^3$) values are observed along the northern and southern tip of the domain. Both the southern and northern part experiences strong northerly drift (LSTR $> 0.7 \times 10^5 \text{ m}^3$), while the central regions experience weak southerly drift (LSTR $< 0.3 \times 10^5 \text{ m}^3$). Based on visual observations, Kumar et al. (2001) estimated a net northward directed LST of $0.6 \times 10^5 \text{ m}^3$ and gross LST of $2 \times 10^5 \text{ m}^3$ using Walton and Bruno Equation (Walton and Bruno, 1989) along Arge beach, Karwar. Kumar et al. (2003) measured the lateral and vertical distribution of LSTR with traps deployed in the surf zone along the Karwar from February to May 1990. They reported LSTR values ranging from -1532 to 1396 m^3/day with an average gross transport rate of 726 m^3/day . They also reported a predominant northward direction of LST. In the present study, the averaged LSTR from February to May varies from -500 to 1400 m^3/day , with an average gross value ranging from 300 to 1200 m^3/day across the whole domain (Figure not shown).

Most of the regions in the Honnavar domain (Figure 9d) experiences a predominant northerly drift. Previously, Chempalayil et al. (2014) reported that about 84% of the time, a northerly drift was observed along this domain. The gross LSTR varies from $0.1-1.9 \times 10^5 \text{ m}^3$, and the net LSTR ranges from -0.8 to $1.9 \times 10^5 \text{ m}^3$ (Table 3).

A comparison of gross LST rates for seven days during calm (non-monsoon), monsoon, and cyclone conditions along the four selected stretches are shown in Figure 10, and daily averaged wave characteristics during the same period for all three conditions are shown in Figure 11. During the calm conditions, the largest gross LST rates are observed along the Ganpatipule coast (up to 1520 m^3/day). The largest gross rate of $\sim 5700 \text{ m}^3$ for seven days is observed along the Ganpatipule coast, followed by Honnavar, where the gross LST rate is $\sim 2660 \text{ m}^3$ with a large variation in LST rate of more than 50%. Both Vengurla and Karwar experiences the least gross rates ($\sim 1200 \text{ m}^3$) during calm conditions, and the variations are less than 5%. Results suggest that during calm conditions, the presence of north-westerly waves along the Ganpatipule coast (Figure 11a) and south-westerly swells along the Honnavar (discussed in the previous session) drives the larger LST rates.

During monsoon, Karwar experiences larger gross LST rates (exceeding 3800 m³/day), and total gross LST rates during the seven days are about ~20140 m³. Honnavar experiences a maximum gross LST rate of 2660 m³/day and the gross LST rate during the seven days is ~11400 m³. The least LST rates are observed along the Ganpatipule region, where the LST rates oscillate between 760 and 1140 m³, followed by Vengurla, where the LST rates oscillate between 1140 and 1900 m³.

However, when the Ockhi cyclone occurred, the LST rates are higher along all four stretches ranging from 760 to 6270 m³, and the maximum LST rates observed along Honnavar, Karwar, and Vengurla is on 3 December. At Ganpatipule, the maximum LST is observed on 4 December, and the least gross rates during the seven days of cyclone event are along this region (~10260 m³).

During the monsoon, the high wind speed persists for longer period and resulted in high waves, whereas the high winds during the cyclone is for few days and hence the wave heights are less than that during the monsoon (Figure 11b). Larger LST rates are observed during a cyclone condition in the CWCI in comparison with calm and monsoon conditions. This is clearly due to the incident wave direction during the cyclone period, where waves ranging from 4-8 s generally approach the domain predominantly from the southwest (Figure 11c) with a larger breaker angle, thus generating large LST. In contrast, during monsoon, the waves with a period ranging from 6-8 s approach the domain almost perpendicular to the coast, with small breaker angles, and generate small LST compared to the cyclone period (Figure 11b). A comparison of gross LST rates along the Vengurla region during pre-monsoon, monsoon, and two cyclone events of two different years (Ockhi cyclone in 2017 and Kyarr cyclone in 2019) are shown in Table 4. It is observed that both the cyclones that lasted for few days generated ~40% of the LST generated during an entire calm season. Interestingly, Cyclone Kyarr generates LST rates up to 16% of that year's entire monsoon-induced LST rates. This suggests that the sediment budgets along the CWCI are undoubtedly altered by cyclone conditions which last for a few days. Hence, while planning and designing coastal protection measures or coastal structures along CWCI, one should consider the cyclone cases, as continued anthropogenic forcing will amplify the risk of cyclones in the Arabian Sea (Murakami et al., 2017).

4. Conclusion

The present study examines the spatial distribution of wave characteristics and associated littoral drift patterns along the CWCI. This is the first kind of study attempted along the entire CWCI, employing a wave transformation numerical model with time and space varying measured data as input. The model performance is compared with the measured data at 9 m and 5 m water depth during monsoon and non-monsoon periods. Statistical analysis suggests that the model has succeeded in

replicating the wave conditions in the nearshore waters. Across the study domain, during pre-monsoon, H_s intensity is higher along the southern and northern regions than the central regions, whereas during post-monsoon, only the southern region experiences larger waves compared with other areas. The period generally varies in the range of 4-6 s across the whole domain during both seasons, with predominant south-south-westerly waves in the southern region and north-westerly waves in the northern region. During monsoon, the domain experiences an average H_s in the range of 1-2 m with a period ranging from 5-7 s with a predominant wave direction of west-southwest ($\sim 250-260^\circ$). The wave energy fluxes along the 10 m water depth of CWCI are predominantly directed towards the south in the northern part of CWCI. In contrast, along the southern and central regions, they are directed towards the north. The distribution of nearshore wave characteristics and LST rates along the selected stretches in the CWCI is also examined. It is observed that along the breaker zone, the difference in the intensity of H_s along the northern and southern parts of CWCI is relatively low ($\sim 3\%$). Among the four stretches, Karwar experiences lower gross LSTR ($0.03 - 0.38 \times 10^6 \text{ m}^3/\text{yr}$) than other regions, while Honnavar experiences more ($0.038 - 0.72 \times 10^6 \text{ m}^3/\text{yr}$). All stretches experience a net northerly drift, except Ganpatipule, where the net drift is towards the south. Our analysis also suggests that the monsoon impact on the sea states of the nearshore regions of CWCI is larger than the cyclone Ockhi impacts. However, during cyclone Kyarr, the maximum H_s observed along nearshore waters of the Vengurla are similar to the values in the monsoon. On the other hand, we also observed that the two recent cyclones that lasted for few days in the Arabian Sea generated $\sim 40\%$ of the LST generated during an entire calm season, and thus sediment budgets along the CWCI will transform in the near future due to the increase in the frequency of cyclonic storms in the Arabian Sea (Murakami et al., 2017).

Acknowledgements

The Director, CSIR-National Institute of Oceanography, Goa encouraged to carry out the study. The wave measurement at Vengurla was supported by the Council of Scientific & Industrial Research, New Delhi, whereas that at Ratnagiri and Karwar was supported by the Ministry of Earth Sciences through INCOIS, Hyderabad. This work forms part of the Ph.D. thesis of the first author registered at Bharathidasan University, Tiruchirappalli. This is NIO contribution xxxx.

References

- Aboobacker, V.M., Vethamony, P., Rashmi, R., 2011. 'Shamal' swells in the Arabian Sea and their influence along the west coast of India. *Geophys. Res. Lett.* 38(3): L03608. <https://doi.org/10.1029/2010GL045736>
- Amrutha, M.M., Kumar, V.S., George, J., 2017. Observations of long-period waves in the nearshore waters of central west coast of India during the fall inter-monsoon period. *Ocean Eng.* 131, 244–262. <https://doi.org/10.1016/j.oceaneng.2017.01.014>
- Amrutha, M.M., Kumar, V.S., Sandhya, K.G., Nair, T.M.B., Rathod, J.L., 2016a. Wave hindcast studies using SWAN nested in WAVEWATCH III - Comparison with measured nearshore buoy data off Karwar, eastern Arabian Sea. *Ocean Eng.* 119, 114–124. <https://doi.org/10.1016/j.oceaneng.2016.04.032>
- Amrutha, M.M., Sanil Kumar, V., Singh, J., 2016b. Changes in nearshore waves during the active sea/land breeze period off Vengurla, central west coast of India. *Ann. Geophys.* 34, 215–226. <https://doi.org/10.5194/angeo-34-215-2016>
- Anderson, D., Ruggiero, P., Antolínez, J.A.A., Méndez, F.J., Allan, J., 2018. A Climate Index Optimized for Longshore Sediment Transport Reveals Interannual and Multidecadal Littoral Cell Rotations. *J. Geophys. Res. Earth Surf.* 123, 1958–1981. <https://doi.org/10.1029/2018JF004689>
- Anoop, T.R., Kumar, V.S., Shanas, P.R., Johnson, G., 2015. Surface wave climatology and its variability in the north Indian Ocean Based on ERA-interim re-analysis. *J. Atmos. Ocean. Technol.* 32, 1372–1385. <https://doi.org/10.1175/JTECH-D-14-00212.1>
- Anoop, T.R., Sanil Kumar, V., Shanas, P.R., 2014. Spatial and temporal variation of surface waves in shallow waters along the eastern Arabian Sea. *Ocean Eng.* 81, 150–15. <https://doi.org/10.1016/j.oceaneng.2014.02.010>
- Anoop, T.R., Shanas, P.R., Aboobacker, V.M., Kumar, V.S., Nair, L.S., Prasad, R., Reji, S., 2020. On the generation and propagation of Makran swells in the Arabian Sea. *Int. J. Climatol.* 40, 585–593. <https://doi.org/10.1002/joc.6192>
- Barstow, S.F., Kallstad, T., 1991. Field trials of the directional waverider. in: *Proceedings of the First International Offshore and Polar Engineering Conference, Edinburgh, III*, 55–63.
- Chandramohan, P., Sanil Kumar, V., Nayak, B.U., Pathak, K., 1993. Variation of longshore current and sediment transport along the south Maharashtra coast, west coast of India. *Indian J. Mar. Sci.* 22, 115–118.
- Chempalayil, S.P., Kumar, V.S., Dora, G.U., Johnson, G., 2014. Near shore waves, long-shore currents and sediment transport along micro-tidal beaches, central west coast of India. *Int. J. Sediment Res.* 29, 402–413. [https://doi.org/10.1016/S1001-6279\(14\)60054-8](https://doi.org/10.1016/S1001-6279(14)60054-8)
- Chowdhury, P., Behera, M.R., 2017. Effect of long-term wave climate variability on longshore sediment transport along regional coastlines. *Prog. Oceanogr.* 156, 145–153. <https://doi.org/10.1016/j.pocan.2017.06.001>

- Dora, G.U., Kumar, V.S., 2015. Sea state observation in island-sheltered nearshore zone based on in situ intermediate-water wave measurements and NCEP/CFSR wind data. *Ocean Dyn.* 65, 647-663. <https://doi.org/10.1007/s10236-015-0822-1>
- Dora, G.U., Kumar, V.S., 2018. Hindcast of breaking waves and its impact at an island sheltered coast, Karwar. *Ocean Dyn.* 68, 1-16. <https://doi.org/10.1007/s10236-017-1112-x>
- George, J., Kumar, V.S., 2019. Long-term variations in nearshore wave climate and littoral drift at Ganpatipule coast, eastern Arabian Sea and its link to Pacific climate variability. *J. Geophys. Res. Ocean.* 124, 7307-7327. <https://doi.org/10.1029/2018JC014900>
- George, J., Kumar, V.S., 2020. Climatology of wave period in the Arabian Sea and its variability during the recent 40 years. *Ocean Eng.* 216, Article number 108014. <https://doi.org/10.1016/j.oceaneng.2020.108014>
- George, J., Kumar, V.S., Gowthaman, R., Singh, J., 2020. Nearshore waves and littoral drift along a micro-tidal wave-dominated coast having comparable wind-sea and swell energy. *J. Mar. Sci. Eng.* 8, 55. <https://doi.org/10.3390/JMSE8010055>
- George, J., Sanil Kumar, V., Victor, G., Gowthaman, R., 2019. Variability of the local wave regime and the wave-induced sediment transport along the Ganpatipule coast, eastern Arabian Sea. *Reg. Stud. Mar. Sci.* 31, Article number 100759. <https://doi.org/10.1016/j.rsma.2019.100759>
- Hydraulics, W.L.D., 2006. *Delft3D User Manual*. Published and printed by Deltares, The Netherlands.
- Kamphuis, J.W., 1991. Alongshore sediment transport rate. *J. Waterw. Port Coast. Ocean Div. ASCE* 117 (6), 624-641
- Kankara, R.S., Ramana Murthy, M. V., Rajeevan, M., 2018. National assessment of shoreline changes along India coast-Status report for 26 years 1990-2016. NCCR publication. <http://www.nccr.gov.in>
- Kumar, V.S., Anand, N.M., Chandramohan, P., Naik, G.N., 2003. Longshore sediment transport rate - Measurement and estimation, central west coast of India. *Coast. Eng.* 48, 95-109. [https://doi.org/10.1016/S0378-3839\(02\)00172-2](https://doi.org/10.1016/S0378-3839(02)00172-2)
- Kumar, V.S., George, J., 2016. Influence of Indian summer monsoon variability on the surface waves in the coastal regions of eastern Arabian Sea. *Ann. Geophys.* 34, 871-885. <https://doi.org/10.5194/angeo-34-871-2016>
- Kumar, V.S., George, J., Dora, U., Naseef, M., 2019. Surface wave dynamics off Mumbai coast, north-eastern Arabian Sea. *Ocean Dyn.* 69, 29-42. <https://doi.org/10.1007/s10236-018-1230-0>
- Kumar, V.S., Johnson, G., Udhaba Dora, G., Chempalayil, S.P., Singh, J., Pednekar, P., 2012. Variations in nearshore waves along Karnataka, west coast of India. *J. Earth Syst. Sci.* 121, 393-403. <https://doi.org/10.1007/s12040-012-0160-3>
- Kumar, V.S., Pathak, K.C., Pednekar, P., Raju, N.S.N. and Gowthaman, R., 2006, Coastal processes along the Indian coastline, *Current science*, 91, 530-536
- Kumar, V.S., Raju, N.S.N., Pathak, K.C. and Anand, N.M., 2001, Nearshore processes along North Karnataka coast, *Proceedings International Conference in Ocean Engineering-2001 held at Indian Institute of Technology Madras, Chennai-600 036 during 11-14 December, 2001, Vol. 2, 451-458.*

- Longuet-Higgins, M.S., 1970. Longshore currents generated by obliquely incident sea waves: 2. *J. Geophys. Res.* 75, 6790–6801. <https://doi.org/10.1029/JC075i033p06790>
- McCarroll, R.J., Masselink, G., Wiggins, M., Scott, T., Billson, O., Conley, D.C., Valiente, N.G., 2019. High-efficiency gravel longshore sediment transport and headland bypassing over an extreme wave event. *Earth Surf. Process. Landforms.* 44, 2720-2727. <https://doi.org/10.1002/esp.4692>
- Murakami, H., Vecchi, G.A., Underwood, S., 2017. Increasing frequency of extremely severe cyclonic storms over the Arabian Sea. *Nat. Clim. Chang.* 7, 885-889. <https://doi.org/10.1038/s41558-017-0008-6>
- Noujas, V., Kankara, R.S., Rasheed, K., 2018. Estimation of Longshore Sediment Transport Rate for a Typical Pocket Beach Along West Coast of India. *Mar. Geod.* 41, 201-216. <https://doi.org/10.1080/01490419.2017.1422818>
- Odériz, I., Silva, R., Mortlock, T.R., Mendoza, E., 2020. Climate drivers of directional wave power on the Mexican coast. *Ocean Dyn.* 70, 1253-1265. <https://doi.org/10.1007/s10236-020-01387-z>
- Remya, P.G., Kumar, B.P., Srinivas, G., Nair, T.M.B., 2020. Impact of tropical and extra tropical climate variability on Indian Ocean surface waves. *Clim. Dyn.* 54, 4919-4933. <https://doi.org/10.1007/s00382-020-05262-x>
- Shanas, P.R., Sanil Kumar, V., 2014. Coastal processes and longshore sediment transport along Kundapura coast, central west coast of India. *Geomorphology* 214, 436–451. <https://doi.org/10.1016/j.geomorph.2014.02.027>
- Shanas, P.R., Sanil Kumar, V., 2014. Temporal variations in the wind and wave climate at a location in the eastern Arabian Sea based on ERA-Interim re-analysis data. *Nat. Hazards Earth Syst. Sci.* 14, 1371-1381. <https://doi.org/10.5194/nhess-14-1371-2014>
- USACE, 1984. Shore Protection Manual. Coastal Engineering Research Center (CERC), Dept. of the Army, U.S. Army Corps of Engineers, Washington.
- Walton Jr, T.L., Bruno, R.O., 1989. Longshore Transport at a Detached Breakwater, Phase II, 679-691. <http://www.jstor.org/stable/4297599>.

Table 1. Seasonal averaged significant wave height and wave period ranges distributed along the four stretches and their predominant wave directions during each season

Significant wave height (Hs) range (m)				
Season	Ganpatipule	Vengurla	Karwar	Honnavar
Pre-monsoon	0.2-0.8	0.4-0.7	0.2-0.7	0.1-0.8
Monsoon	0.6-1.8	1.2-1.7	0.6-2.0	0.1-1.9
Post-monsoon	0.3-0.6	0.4-0.7	0.2-0.7	0.1-0.8
Wave period range (s)				
Pre-monsoon	4.0-5.0	4.0-6.0	4.0-6.0	4.0-6.0
Monsoon	5.0-7.0	6.0-7.0	6.0-7.0	6.0-7.0
Post-monsoon	3.0-5.0	4.0-6.0	4.0-6.0	4.0-6.0
Predominant wave direction (Deg)				
Pre-monsoon	220-280	220-260	220-300	230-250
Monsoon	235-270	230-240	240-250	250-260
Post-monsoon	220-280	220-260	220-300	230-250

Table 2. Significant wave height and period ranges distributed along the nearshore water (at 4 m water depth) of four stretches and their predominant wave directions during each season

Significant wave height (Hs) range (m)				
Season	Ganpatipule	Vengurla	Karwar	Honnavar
Pre-monsoon	0.18-1.9	0.13-1.9	0.13-1.9	0.2-1.9
Monsoon	0.3-2.3	0.4-2.3	0.4-1.9	0.5-2.0
Post-monsoon	0.19-2.0	0.13-1.9	0.13-1.9	0.2-1.9
Wave period range (s)				
Pre-monsoon	2.4-6.9	2.6-7.9	2.7-9.0	2.8- 8.9
Monsoon	3.4-8.5	3.3-9.1	3.8-9.3	3.0-9.0
Post-monsoon	2.5-8.0	2.6-7.9	2.7-9.0	2.9-9.5
Predominant wave direction (Deg)				
Pre-monsoon	226-255	220-250	220-255	225-250
Monsoon	250-260	245-255	245-260	242-255
Post-monsoon	220-255	220-250	220-255	225-250

Table 3. Gross and net longshore sediment transport (LST) ranges for the four stretches

	LSTR range			
	Ganpatipule	Vengurla	Karwar	Honnavar
Gross ($\times 10^5 \text{ m}^3$)	0.1-1.2	0.1-1.5	0.1-1.0	0.1-1.9
Net ($\times 10^5 \text{ m}^3$)	-1.1-1.0	-1.1-1.4	-0.4-1.0	-0.8 - 1.9

Table 4. LST rates along the Vengurla coast during different seasons and cyclone conditions during 2017 and 2019

LST (m³)	2017	2019
Pre-monsoon	27402	48230
Monsoon	116775	113906
Cyclone event	10744	18260
Total Gross (yearly)	168767	208561

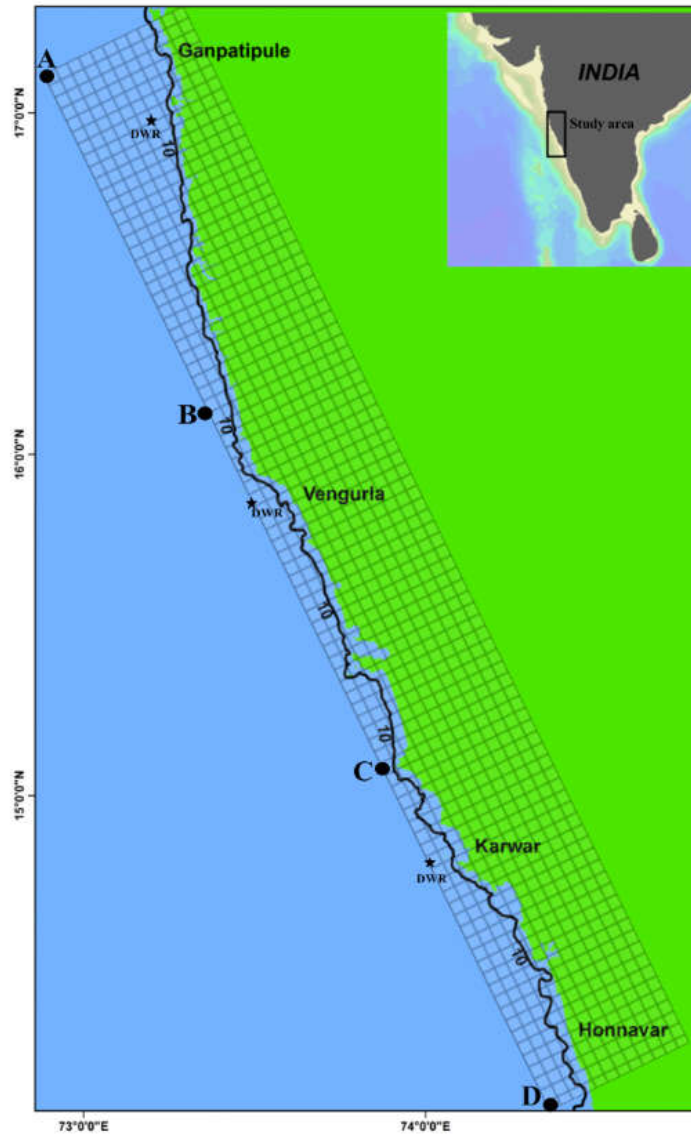


Figure 1. The study region in the Arabian Sea is shown in the inside figure. The outer figure is the study domain of the central west coast of India. The rectangular box represents the model grid and its boundaries. Wave buoy locations are indicated as DWR. Thick line is the 10 m depth contour

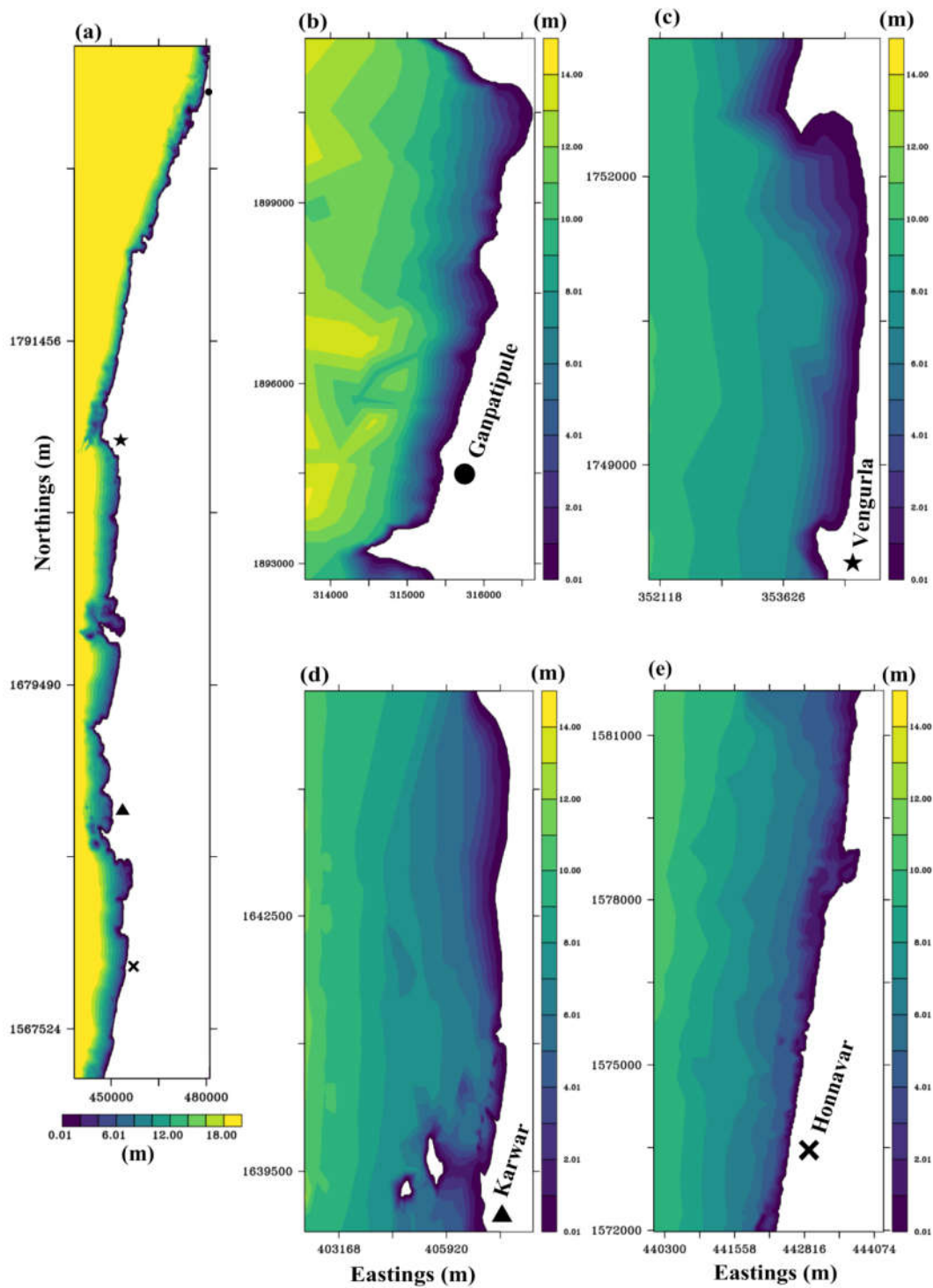


Figure 2. Bathymetry interpolated study domain along (a) the central west coast of India and the selected stretches of (b) Ganpatipule (c) Vengurla (d) Karwar and (e) Honnavar used in the wave transformation model

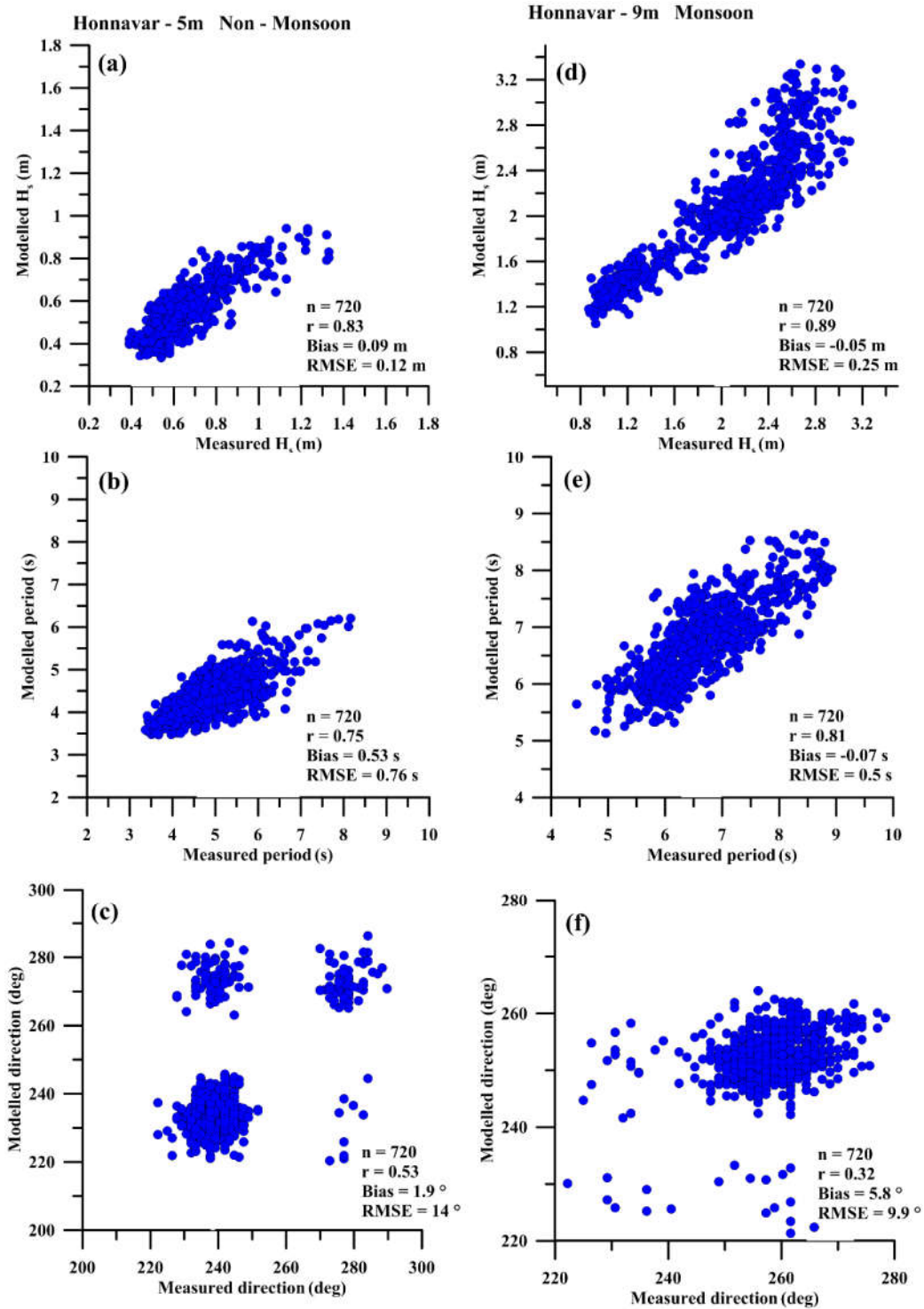


Figure 3. Scatter plots of significant wave height, period and direction between the model simulation and measured data during a non-monsoon month (at 5 m) and monsoon month (at 9 m).

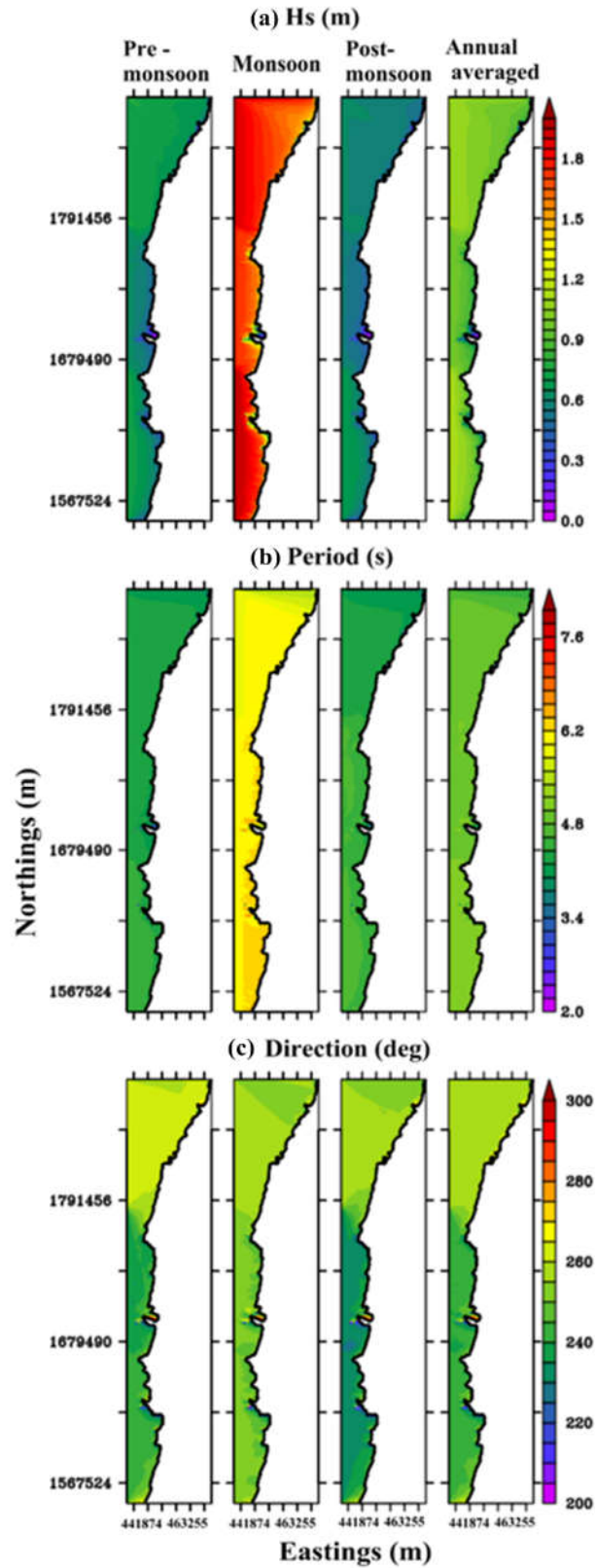


Figure 4. Spatial distribution of (a) significant wave height, (b) period, and (c) direction during seasonal and annual averaged scales along the central west coast of India

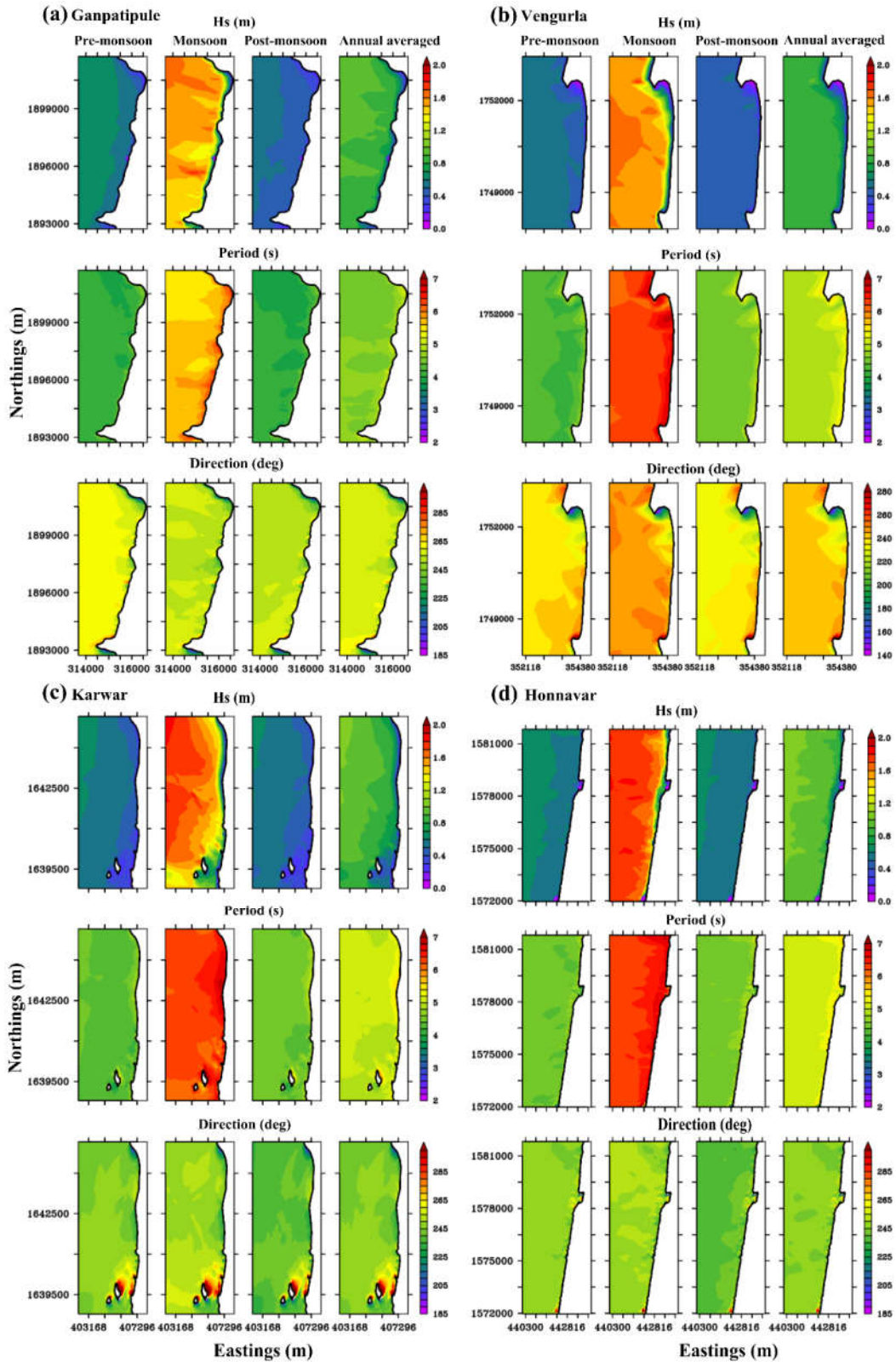


Figure 5. Spatial distribution of significant wave height, period, and direction during seasonal and annual averaged scales along the selected stretches in the central west coast of India

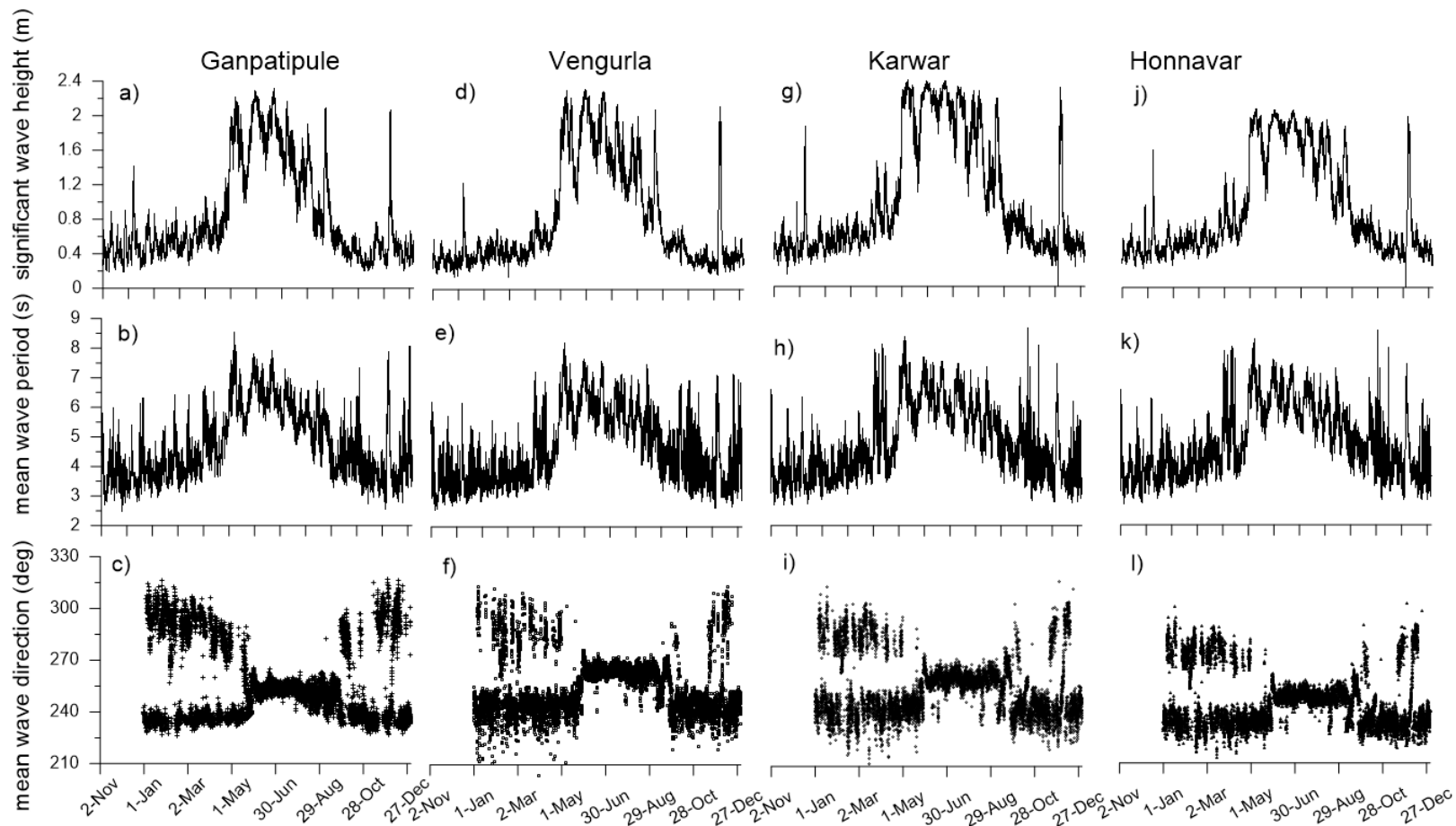


Figure 6. Time series of wave characteristics at 4 m water depth along different locations

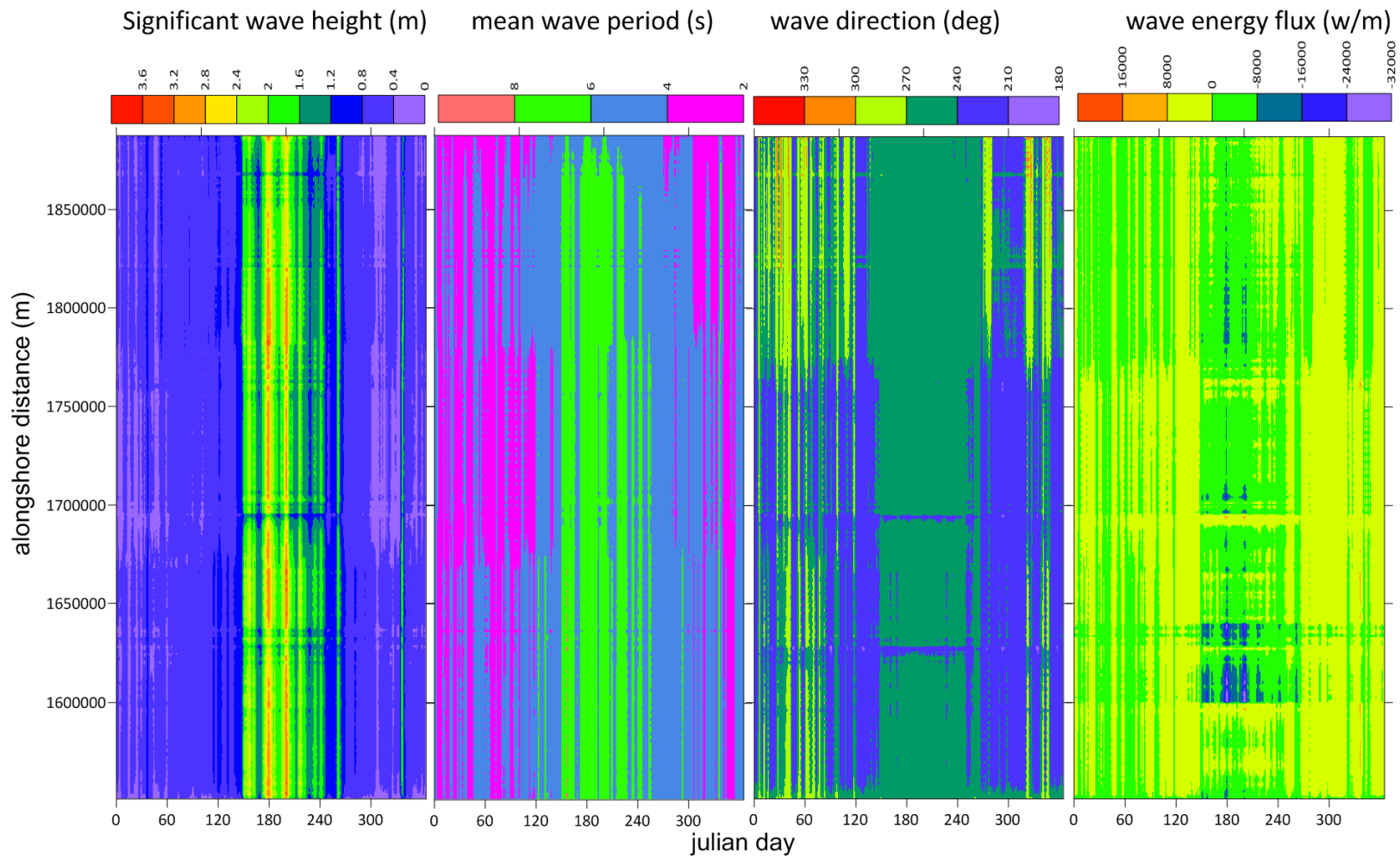


Figure 7. Hovmoller diagram (time and alongshore distance) of significant wave height, mean wave period, wave direction and wave energy flux at 10 m water depth along the central west coast of India

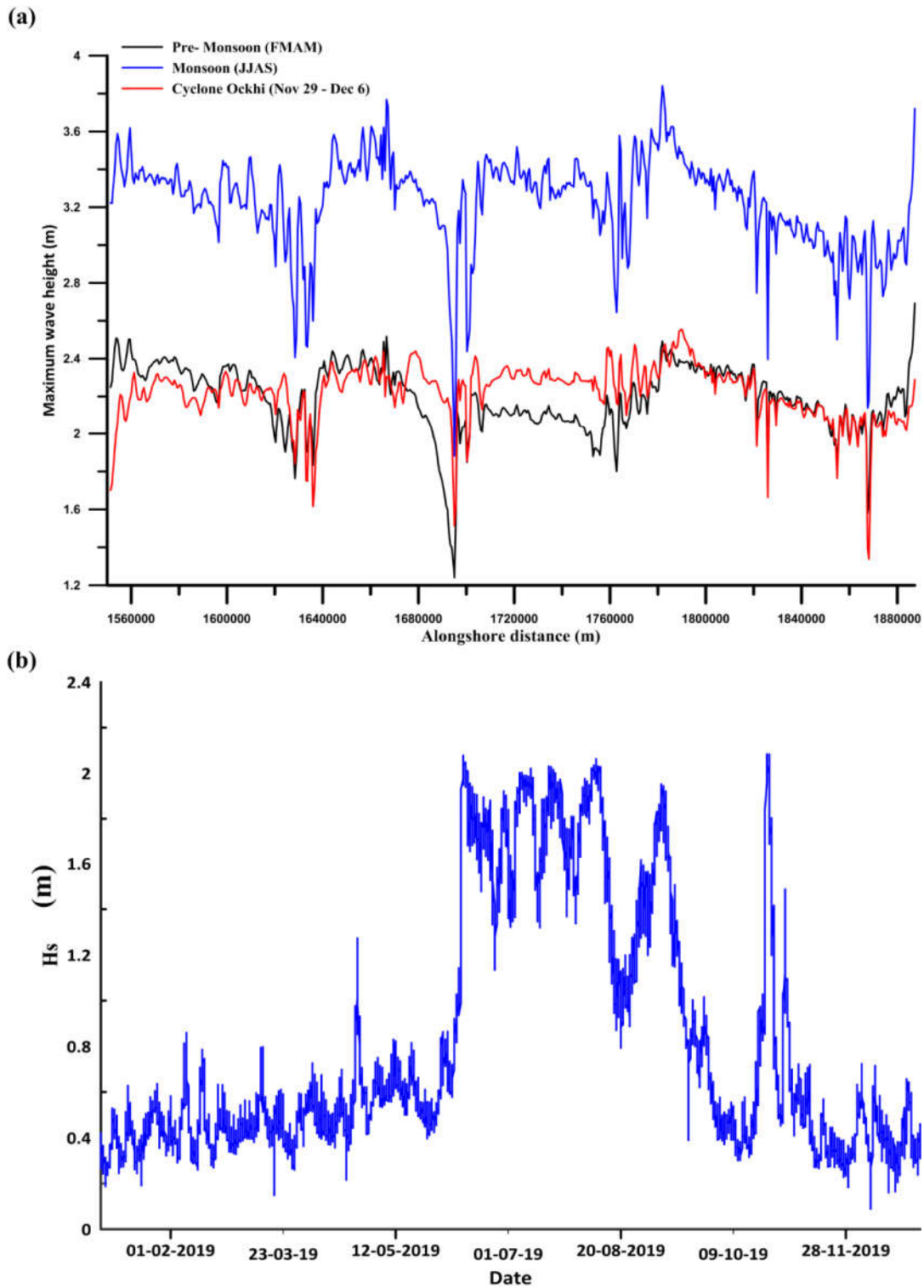


Figure 8 (a) Maximum wave height observed in the domain during a pre-monsoon (calm) season, monsoon season, and cyclone event (b) time series of H_s at 4 m water depth along the Vengurla during 2019

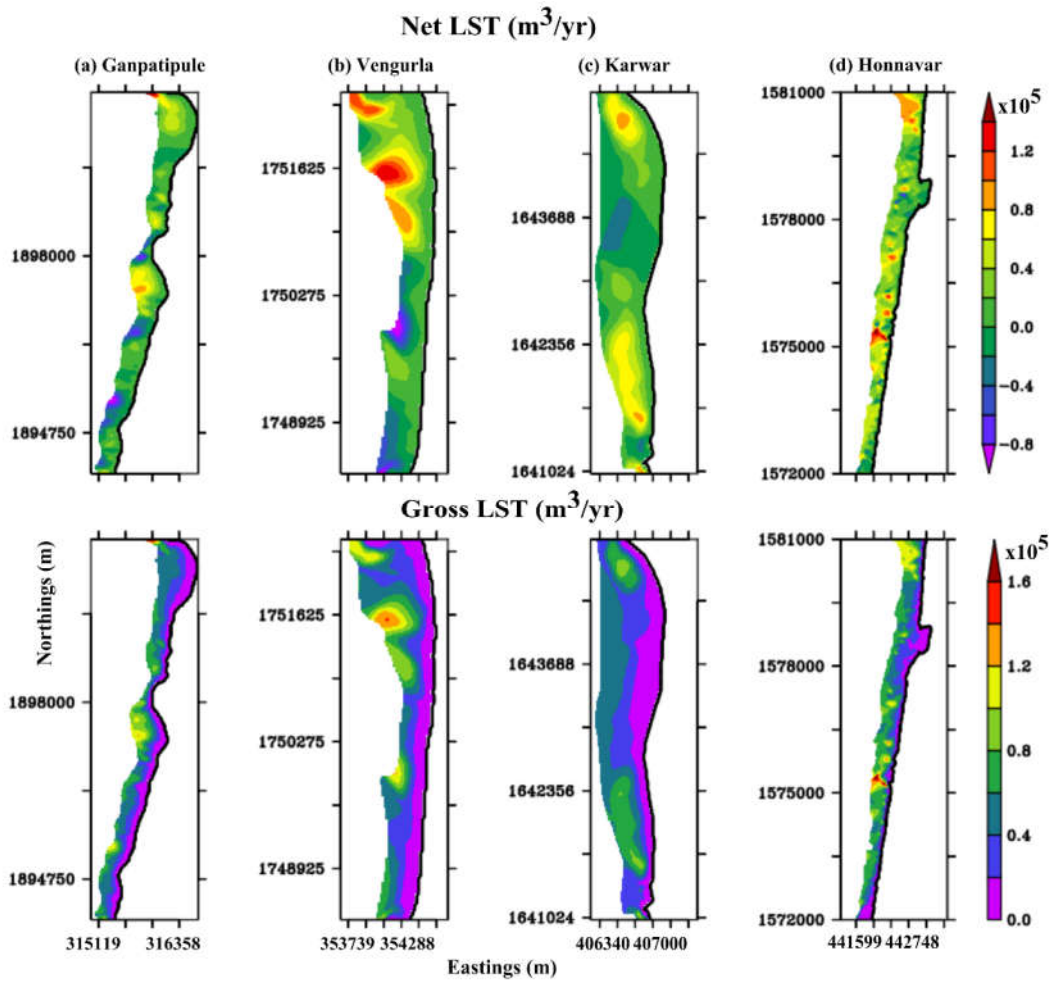


Figure 9. Spatial distribution distribution of longshore sediment transport (LST) rates along selected stretches. Top panel shows the annual net LST and bottom panel shows the annual gross LST

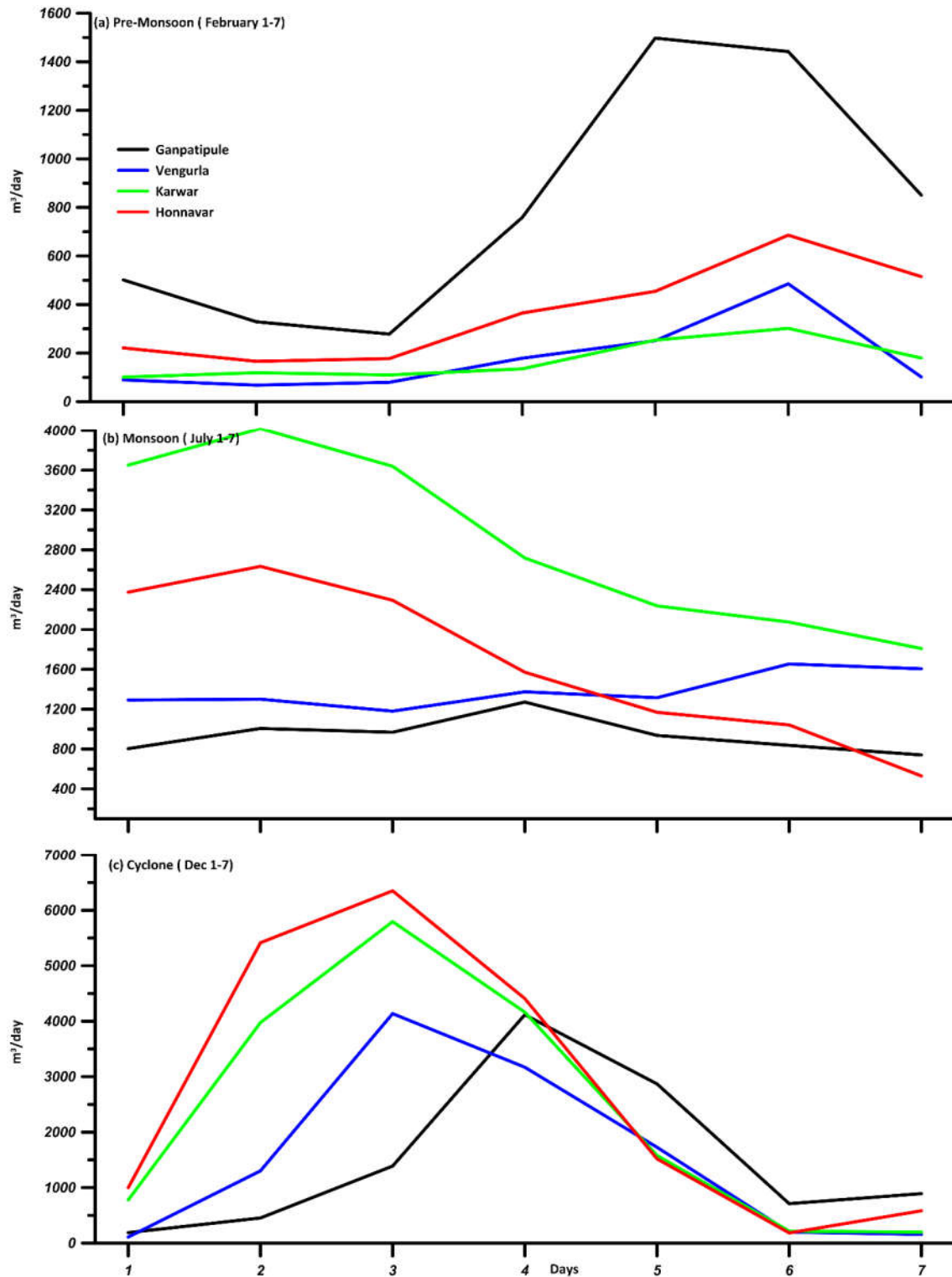


Figure 10. Gross longshore sediment transport rates along selected stretches for seven days each during a non-monsoon (calm), monsoon, and cyclone event

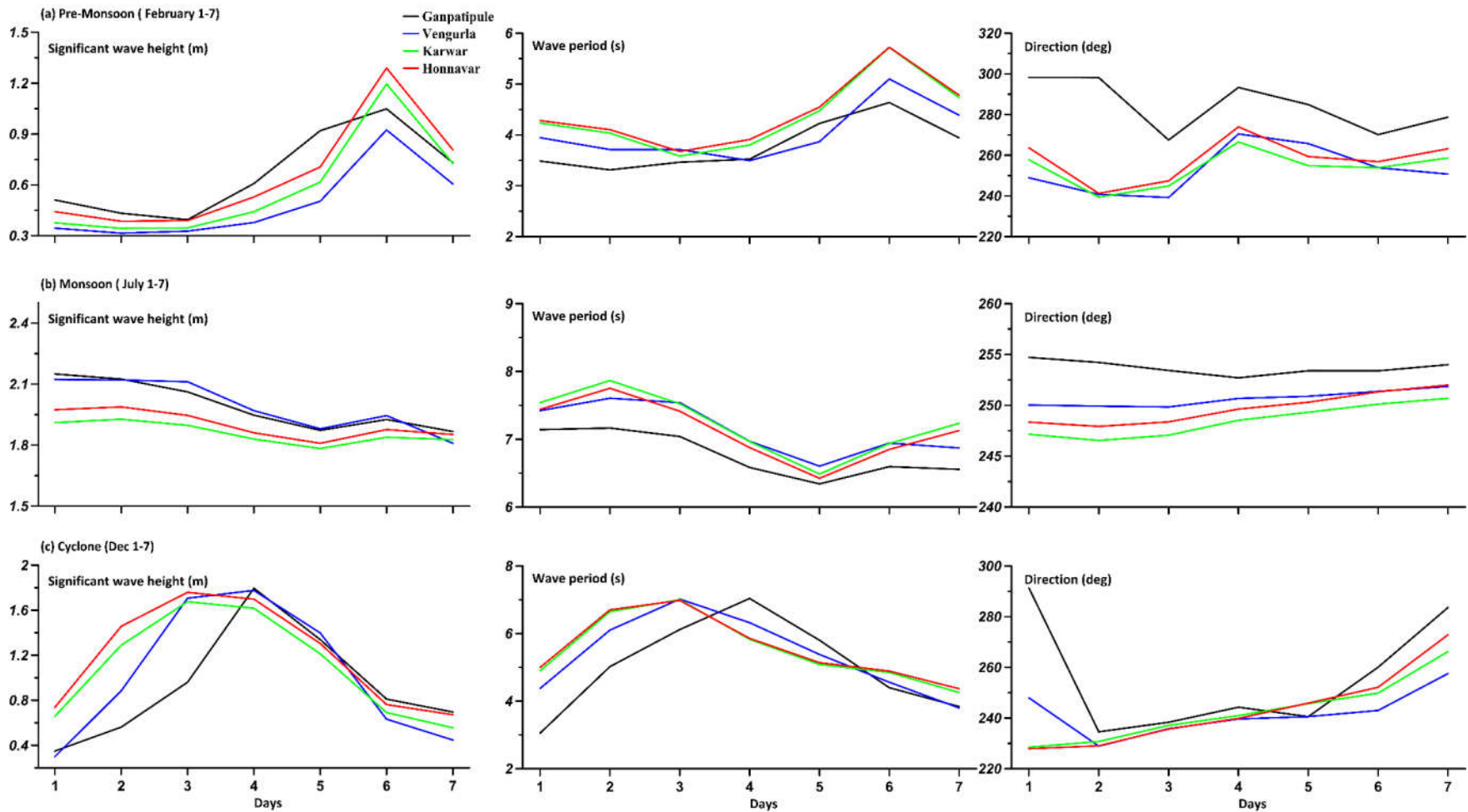


Figure 11. Daily averaged wave characteristics along selected stretches for seven days each during a non-monsoon (calm), monsoon and cyclone event